Available online at www.sciencedirect.com
SCIENCE DIRECT®
Geochimica et Cosmochimica Acta 70 (2006) 323–336
Geochimica
www.elsevier.com/locate/gca

The effect of iron on montmorillonite stability. (II) Experimental investigation

James Wilson [a,b,c,*], Gordon Cressey [c], Barbara Cressey [d], Javier Cuadros [c], K. Vala Ragnarsdottir [b], David Savage [e], Masahiro Shibata [f]

[a] *Chemical Hazards and Poisons Division (London), Health Protection Agency, Medical Toxicology Unit, Avonley Road, London SE14 5ER, UK*
[b] *Department of Earth Sciences, University of Bristol, Wills Memorial Building, Queen's Road, Bristol, BS8 1RJ, UK*
[c] *Department of Mineralogy, The Natural History Museum, Cromwell Road, London SW7 5BD, UK*
[d] *School of Chemistry, University of Southampton, SO17 1BJ, UK*
[e] *Quintessa Ltd. 24 Trevor Road, West Bridgford, Nottingham NG2 6FS, UK*
[f] *Japan Nuclear Cycle Development Institute, Tokai-mura Prefecture, Japan*

Received 8 November 2004; accepted in revised form 7 September 2005

Abstract

Several designs proposed for high-level nuclear waste (HLW) repositories include steel waste canisters surrounded by montmorillonite clay. This work investigates montmorillonite stability in the presence of native Fe, magnetite and aqueous solutions under hydrothermal conditions. Two series of experiments were conducted. In the first, mixtures of Na-montmorillonite, magnetite, native Fe, calcite, and NaCl solutions were reacted at 250 °C, P_{sat} for between 93 and 114 days. In the second series, the starting mixtures included Na-montmorillonite, native Fe and solutions of $FeCl_2$ which were reacted at temperatures of 80, 150, and 250 °C, P_{sat}, for 90–92 days. Experiments were analysed using XRD, FT-IR, TEM, ICP-AES, and ICP-MS. In the first series of experiments, native Fe oxidised to produce magnetite and the starting montmorillonite material was transformed to Fe-rich smectite only when the Fe was added predominantly as Fe metal rather than Fe oxide (magnetite). The Fe-rich smectite was initially Fe(II)-rich, which oxidised to produce an Fe(III)-rich form on exposure to air. The expansion of this material on ethylene glycol solvation was much reduced compared to the montmorillonite starting material. TEM imaging shows that partial loss of tetrahedral sheets occurred during transformation of the montmorillonite, resulting in adjacent layers becoming H-bonded with a 7 Å repeat. The reduced swelling property of the Fe-smectite product may be due predominantly to the structural disruption of smectite layers and the formation of H-bonds. Solute activities corresponded to the approximate stability field calculated for hypothetical Fe(II)-saponite. In the second series of experiments, significant smectite alteration was only observed at 250 °C and the product contained a small proportion of a 7 Å repeat structure, observable by XRD. In these experiments, solute activities coincide with berthierine. The experiments indicate that although bentonite is still a desirable choice of backfill material for HLW repositories, some loss of expandability may result if montmorillonite is altered to Fe-rich smectite at the interface between steel canisters and bentonite.

1. Introduction

Most experimental investigations into the stability of smectite under expected conditions of geological disposal of high level waste (HLW) have focused on the nature and kinetics of the smectite to illite conversion (e.g., Whitney and Northrop, 1988; Huang et al., 1993; Cuadros and Linares, 1996). In the first paper of this two paper set (Wilson et al., 2006), it was noted that observations of geological systems do not provide a clear indication of the potential for montmorillonite alteration to Fe-rich sheet silicates in HLW repositories, resulting in a need for thermochemical modelling (Wilson et al., 2006) and experimental data (this paper). The aim of the experiments presented

* Corresponding author.
E-mail address: James.Wilson@HPA.org.uk (J. Wilson).

0016-7037/$ - see front matter © 2006 Published by Elsevier Inc.
doi:10.1016/j.gca.2005.09.023

in this paper is to provide some preliminary data on the nature of montmorillonite interactions with iron, and to determine whether the models of Fe-rich clay mineral stability presented by Wilson et al. (2006) predict pathways of clay mineral alteration.

The synthesis conditions that favour Fe-rich sheet silicate formation (Harder, 1976, 1978; Decarreau and Bonnin, 1986) suggest that reducing conditions and low silica activities promote the formation of dioctahedral and trioctahedral Fe-rich smectite. Few experimental data on Fe–bentonite interactions have been reported in the literature. Müller-Vonmoos et al. (1991) conducted experiments on compacted mixtures of bentonite–magnetite which were discussed by Madsen (1998). The lack of mineralogical alteration observed was probably a result of the low temperatures at which the experiments were conducted (80 °C). To our knowledge, the only experiments in the literature at the time of writing that are similar to those reported here, are by Guillaume et al. (2003, 2004) who conducted experiments at 300 °C to produce trioctahedral Fe-rich clay and also observed significant chloritisation of smectite in experiments that included a plate of native Fe.

Our study differs from those of Guillaume et al. (2003, 2004) in several ways. We used a more smectite-rich material (97 wt.% Na-montmorillonite as opposed to 79 wt% Na/Ca-montmorillonite), the smectite we used had a higher layer charge (0.55 as opposed to 0.38 per $O_{10}(OH)_2$), some of our experiments included mixtures with only Fe and montmorillonite, some of them were conducted with $FeCl_2$, some with NaCl solutions, some with calcite and we used a higher solution:bentonite mass ratio (66.7 as opposed to 10). We also report additional insights on the alteration using high resolution TEM and our results were interpreted using thermodynamic modelling.

2. Methods and materials

2.1. Starting material characterisation

The starting material used in this study was "Kunipia-F" (supplied by the Kunimine Industry, Japan), which is a smectite-enriched fraction of an original bentonite rock. Its XRD pattern is typical of dioctahedral smectite (06, 33 at 1.496 Å) with "turbostratic" layer stacking. Quantitative phase analysis by X-ray diffraction with a position sensitive detector (XRD-PSD) described by Batchelder and Cressey (1998), indicates that the material consists of 97 wt.% smectite, 2 wt.% quartz and 1 wt.% cristobalite. Scanning XRD patterns of oriented air-dry and ethylene glycol solvated mounts of "Kunipia-F" have $d(001)$ maxima with d-values of 12.5 Å in the air-dry state (typical of 1-water layer Na-smectite, e.g., Glaeser and Méring, 1968; MacEwan and Wilson, 1980) and 17 Å in the ethylene glycol solvated state. The $d(001)$ value after K^+ saturation is 11.4 Å. After heating at 300 °C, the K^+-saturated interlayers collapse to 10.1 Å.

The exchangeable cation content of the Kunipia-F smectite starting material was determined by displacing cations with $Cu(EDA)_2^{2+}$ solution (Bergaya and Vayer, 1997). The exchangeable cation content of the Kunipia-F smectite (meq/100 g) is as follows: Na^+, 119.2 ± 2.8; Ca^{2+}, 13.7 ± 0.5; K^+, 1.4 ± 0.1; Mg^{2+}, 0.9 ± 0.03 giving a total cation exchange capacity (CEC), 135 ± 2.8 meq/100 g.

Major element concentrations were determined by X-ray fluorescence (XRF) spectrometric analysis of lithium metaborate glass beads. The Fe(II) content of the material was determined by digestion of samples in hot concentrated H_2SO_4 and HF with subsequent complexing of HF with boric acid and titrating $K_2Cr_2O_7$ against dissolved Fe(II) with diphenylamine sulphonate indicator.

The average half unit cell formula (calculated from major element concentrations after correction for the presence of quartz and cristobalite by subtracting 3%wt of SiO_2), was determined using the method outlined by Moore and Reynolds (1997). The interlayer cation content in the half unit cell formula is in good agreement with the exchangeable cation data

$$(Na_{0.48}Ca_{0.03}K_{0.01})(Al_{1.54}Mg_{0.33}Fe^{3+}{}_{0.09}Fe^{2+}{}_{0.02})(Si_{3.87}Al_{0.13})\,O_{10}(OH)_2{\cdot}nH_2O.$$

The composition of the octahedral sheets according to this formula are also in good agreement with Fourier transform-infrared (FT-IR) analysis of the Kunipia-F material, which indicates that it is primarily montmorillonite (see Fig. 7). The Si–O stretching band at 1038 cm^{-1} is typical of aluminous dioctahedral smectite, as is a broad OH-stretching band centred on 3629 cm^{-1} (Russell and Fraser, 1994) and the bands centred at 624, 522, and 467 cm^{-1}.

2.2. Analytical methods

The bulk mineralogy of each experimental product was determined by XRD (step size of either 0.015 or 0.02 °2θ and a counting time of either 2 or 10 s per step). Preferred orientation mounts were made by dispensing suspensions in deionised water onto glass slides. Ethylene-glycol solvated samples were prepared by exposing air-dry preferred orientation mounts to ethylene glycol vapour for 16 h at a temperature of 60 °C. The positions of smectite (06, 33) peaks were fitted using a combination of symmetric Pearson VII and Lorentzian functions.

Infrared spectra of the starting material and experiments were collected on KBr disks that were heated to 150 °C using a Nicolet 800 Fourier transform infrared (FT IR) spectroscope.

Samples for TEM examination were prepared by standard techniques (grain dispersions supported on carbon films on copper support grids). Images of key samples were obtained using a JEOL JEM 3010 with LaB6 electron source operating at 300 kV. Digital images were captured, processed and recorded using a Gatan Multiscan camera.

Fluids from hydrothermal experiments were analysed for dissolved Ca, Fe, Mg, Na, and Si using a "Ultima" ICP-AES supplied by Jobon-Yvon. Dissolved Al was measured by ICP-MS with a VG Elemental Plasma Quad II instrument. Sample solutions were filtered through 0.2 μ m cellulose nitrate membranes and acidified to 1% v/v HNO_3.

The pH values of solutions from hydrothermal experiments were measured to within ±0.02 units using glass combination electrodes with a Metrohm 713 pH meter under an N_2 atmosphere.

2.3. Experimental apparatus

Hydrothermal experiments were conducted in titanium batch reactor vessels that were heated in aluminium blocks, surrounded by ceramic insulating material and were attached to an orbital shaker mechanism. The vessels were treated with 1 M HNO_3 for 24 h at 200 °C prior to use to give them a chemically inert inner coating of TiO_2.

2.4. Experimental parameters

The weight ratios of native Fe to smectite in both series of experiments were chosen according to the potential reactions of smectite to a 1:1 or chlorite-type structure. Two simplified reaction pathways were considered (Eqs. (1 and 2)). Al is conserved in the reactions.

1. Conversion of montmorillonite to chamosite

$$Na_{0.35}(Al_{1.65}Mg_{0.35})(Si_4)O_{10}(OH)_2 + 5.9H_2O + 4.125Fe^{2+}_{(aq)} \Longleftrightarrow 0.825(Fe_5Al)(Si_3Al)O_{10}(OH)_8 + 1.525SiO_{2(aq)} + 7.2H^+ + 0.35Na^+ + 0.35Mg^{2+} \quad (1)$$

2. Conversion of montmorillonite to berthierine

$$Na_{0.35}(Al_{1.65}Mg_{0.35})(Si_4)O_{10}(OH)_2 + 4.5H_2O + 1.65Fe^{2+}_{(aq)} \Longleftrightarrow 0.825Fe_2Al_2SiO_5(OH)_4 + 3.175SiO_{2(aq)} + 2.25H^+ + 0.35Na^+ + 0.35Mg^{2+} + 2.725H_2O \quad (2)$$

Eqs. (1) and (2) indicate that approximately 4 and 1.7 moles of Fe are required to alter one mole of smectite into chamosite and berthierine, respectively. The total Fe present in the experiments was therefore set so that the molar ratio of Fe (in solid form) to smectite was 4.

Two sets of hydrothermal experiments were conducted (designated as series 1 and 2, Table 1). Series 1 experiments were designed to represent a repository where bentonite in contact with steel (both with and without corrosion) begins to dissolve as groundwater intrudes into the bentonite backfill. The experiments were conducted at 250 °C in order to increase reaction rates, given that clay mineral alteration reactions are often very slow with little alteration being observed over time periods that are logistically feasible for experimental investigations (e.g., Cuadros and Linares, 1996).

High fluid:clay mass ratio (66.7) and small grain sizes were also used to maximise reaction kinetics. In the series 1 experiments, smectite was reacted with combinations of native Fe (325 mesh) and synthetic magnetite (<5 μm grain diameter). The experiments where magnetite was added in larger quantities (560 mg) were designed to represent repository conditions, where steel had undergone a degree of corrosion prior to the onset of clay mineral alteration. Those with 280 mg of magnetite represent a system where steel has corroded to a lesser extent.

Table 1
Experimental parameters

Experiments	T (°C)	P (bars)	Time (days)	Kunipia-F (mg)	Fe (metal) (mg)	Fe_3O_4 (mg)	$CaCO_3$ (mg)	NaCl (mM)	pH (at 23 °C)
Series 1									
1–1	250	39.7	93	750	433	0	0	36	9.73
1–2	250	39.7	93	750	433	0	37.5	36	9.73
1–3	250	39.7	93	750	28	560	0	36	9.73
1–4	250	39.7	93	750	28	560	37.5	36	9.73
1–5	250	39.7	93	750	231	280	0	36	9.73
1–6	250	39.7	93	750	231	280	37.5	36	9.73
1–13	250	39.7	114	750	433	0	0	36	4.15
1–14	250	39.7	114	750	433	0	37.5	36	4.15
1–15	250	39.7	114	750	28	560	0	36	4.15
1–16	250	39.7	107	750	28	560	37.5	36	4.15
1–17	250	39.7	107	750	231	280	0	36	4.15
1–18	250	39.7	107	750	231	280	37.5	36	4.15

Experiments	T (°C)	P (bars)	Time (days)	Kunipia-F (mg)	Fe (metal) (mg)	$FeCl_2$ (mM)	pH (at 25 °C)
Series 2							
2–1	80	1.0	90	750	433	18.0	4.24
2–2	150	4.8	90	750	433	18.0	4.24
2–3	250	39.7	90	750	433	18.0	4.24
2–5	150	4.8	92	750	433	4.5	4.71
2–6	250	39.7	92	750	433	4.5	4.71

In experiments where magnetite was added as the predominant source of Fe, 28 mg of native Fe was included in the starting mixtures to ensure the removal of any dissolved oxygen initially present in the solutions. Some experiments included a small quantity of $CaCO_3$ (5% of the weight of Kunipia-F smectite) given that this is likely to be present in some bentonites used for repository construction and could affect pH conditions and alter mineral stabilities. In these experiments, NaCl solutions were used to maintain Na as the main interlayer cation. The Na^+ concentration used (36 mM) was approximately twice that required to saturate the interlayer sites. In order to determine if initial solution pH had any effect on alteration, the NaCl solutions had two initial pH values (9.73 for experiments 1–6 and 4.15 for experiments 13–18) prior to being added to mineral powders. The higher pH solution was prepared by the addition of concentrated NaOH.

In the series 2 experiments, native Fe was reacted with Na-montmorillonite and $FeCl_2$ solutions. These experiments were designed to produce extreme conditions to favour smectite alteration with high Fe^{2+} activities rather than to simulate repository conditions. It has also been suggested that dissolved Fe may replace Na^+ from smectite layers (Kamei et al., 1999). In experiments 2–1, 2–2, and 2–3, the Fe^{2+} concentration was approximately twice that required to saturate the interlayers, whereas in experiments 4–6, the concentration was sufficient to replace only half of the interlayer sorption sites. These experiments were conducted at 80, 150, and 250 °C. Reaction times of ~3 months were the longest that were logistically feasible.

2.5. Experimental procedure

The pH of NaCl and $FeCl_2$ solutions were measured under ambient atmospheric conditions. Fifty milliliters of solution was dispensed into each batch reactor vessel containing the solids under ambient atmospheric conditions. The vessels were transferred to a glovebox with an inert $N_{2(g)}$ atmosphere and sealed (to minimise $O_{2(g)}$ present in the headspace of the vessels). They were then moved from the glovebox and placed into preheated aluminium blocks of the batch reactor apparatus, which included an orbital shaker mechanism that activated for 3 h a day for the duration of the experiments.

After reaction, the vessels were open under an inert $N_{2(g)}$ atmosphere and the mineral suspensions were transferred into polypropylene centrifuge tubes. The samples were then centrifuged at 18,000 rpm in a fixed angle (45 °) rotor for 60 min and transferred back to the $N_{2(g)}$ atmosphere where the pH of supernatant fluids was immediately measured. Fluids were rapidly filtered through 0.2 μm cellulose nitrate filter membranes and acidified to a concentration of 1% v/v HNO_3 (using analytical grade reagent) for ICP-AES and ICP-MS analysis.

The solid pastes remaining in the centrifuge tubes were stored frozen until analysis. Solids from the series 1 experiments were split into two sub-samples; one of them was repeatedly washed in deionised water until the supernatants were free of Cl^- ($AgNO_3$ test), the other was not washed. Prior to XRD and FT-IR analysis, samples were oven-dried at 110 °C and gently ground in an agate mortar.

It was not possible to conduct XRD or FT-IR analysis under $O_{2(g)}$-free conditions. Sheet silicates rich in Fe(II) such as berthierine and chlorite can be analysed under atmospheric conditions without complete oxidation and loss of structure. In contrast, Fe(II)-rich trioctahedral smectite appears to be unstable under atmospheric conditions and octahedral Fe(II) rapidly oxidises to Fe(III) with lattice contraction in the *b*-axis direction (Kohyama et al., 1973). However, the oxidised version of Fe-rich saponite can, in principle, be identified in the products of hydrothermal experiments since its $d(06,33)$ value (1.54–1.53 Å, e.g., Kohyama et al., 1973) is significantly different from that of the montmorillonite starting material (1.496 Å) and any alteration of smectite octahedral sheets can be detected using FT-IR.

2.6. Thermodynamic considerations

The software module "react" from "The Geochemist's Workbench" (Bethke, 1996) was used to predict solute speciation under experimental conditions and to thermodynamically calculate quartz and magnetite saturation indices. This uses the "Helgeson B-dot" equation to calculate activity coefficients for measured solute concentrations based on a Debye–Hückel type expression (Helgeson, 1969) and employs a database adapted from the 1996 version of the EQ3/6 database (Wolery, 1996). Calculations were made under the assumption that Cl^- was the predominant anion present.

Solute speciation and pH calculation at elevated temperature were conducted at two $f_{O_{2(g)}}$ values, those corresponding to $H_{2(g)}$–$H_2O_{(l)}$ equilibrium and the magnetite–hematite buffer. The results were the same for both conditions. Concentrations of Cl^- were assumed to be static during the course of the experiments.

Solute activity ratios were plotted on models of mineral-fluid equilibria similar to those given by Wilson et al. (2006) for experiments conducted at 250 °C. The diagrams were calculated using the average calculated value of log *a* $SiO_{2(aq)}$ (−3.11). Logarithmic activity diagrams where $\log(a_{Fe^{2+}}/(a_{H^+})^2)$ was plotted against $\log(a_{Mg^{2+}}/(a_{H^+})^2)$ were constructed with $\log(a_{Na^+}/a_{H^+})$ set at a value of 5, which is similar to the values measured in the experiments. Given that analcime was produced in some experiments, activity diagrams were constructed with analcime as the main Na-bearing framework silicate.

Wilson et al. (2006) demonstrate that smectite with octahedral Fe(II) is more likely to be stable than Fe(III) under $f_{O_{2(g)}}$ values equal to or less than those dictated by magnetite–hematite equilibrium. As it is unlikely that the $f_{O_{2(g)}}$

conditions during the experiments exceeded magnetite–hematite equilibrium, activity diagrams include only Fe(II) aluminosilicates.

3. Results

3.1. XRD analysis

3.1.1. XRD analysis of series 1 experiments

Mineral phases in the run products were determined from powder XRD patterns (Table 2). In the first series of experiments, the main reaction products are essentially the same for both initial pH values (Table 1). The experiments that produced significant smectite alteration were those containing larger quantities of native Fe in the starting mixtures and those containing calcite produced analcime. Calcite-free starting mixtures with magnetite (experiments 1–3, 1–15) show only minor alteration of montmorillonite to analcime. In these experiments, the smectite $d(001)$ values in both air dry and ethylene glycol solvated states were the same as the starting material and the positions of 06,33, and 02,11 peaks indicate that the octahedral sheet compositions are the same as the montmorillonite starting material.

The inclusion of calcite in starting mixtures where magnetite was the main source of Fe (experiments 1–4 and 1–16) produced significant alteration of montmorillonite to analcime. These smectite products are slightly different to those where calcite was not added, in that the $d(001)$ reflections are slightly broader and appear to consist of two components at ~14.5 and 12.7 Å, suggesting that some interlayer cations had been replaced by Ca^{2+} (MacEwan and Wilson, 1980). In the glycolated state, this material produced a single 001 peak at 16.9 Å.

Experiments containing large amounts of native Fe, produced altered smectite and magnetite. The addition of calcite also produced analcime in such experiments. XRD analysis indicates that the montmorillonite starting material was transformed from being Al-rich to Fe-bearing. The positions of the 06,33 peak in the products varied depending on whether or not calcite was included in the starting mixtures. Where calcite was not included (experiments 1–1, 1–13) XRD patterns have broad (06,33) maxima, with up to three components: 1.554, 1.531, and 1.499 Å. The first two indicate the presence of Fe-rich octahedral sheet structures, the third is from unaltered montmorillonite (Fig. 1). When these samples were repeatedly washed in deionised water and allowed to dry in air, the intensity of the 1.554 Å peak decreased relative to the 1.531 and 1.499 Å peaks. In contrast, experiments with the same amounts of native Fe and added calcite (1–2 and 1–14) produced smectite with a single 06,33 peak at 1.54 Å, which shifted to 1.53 Å when samples were repeatedly washed in deionised water (Fig. 2). In addition, a small shoulder was observed near the base of the magnetite 440 peak at ~62 °2θ (1.49 Å) which could indicate that montmorillonite alteration was not complete. In the experiments where similar amounts of both magnetite and Fe were reacted

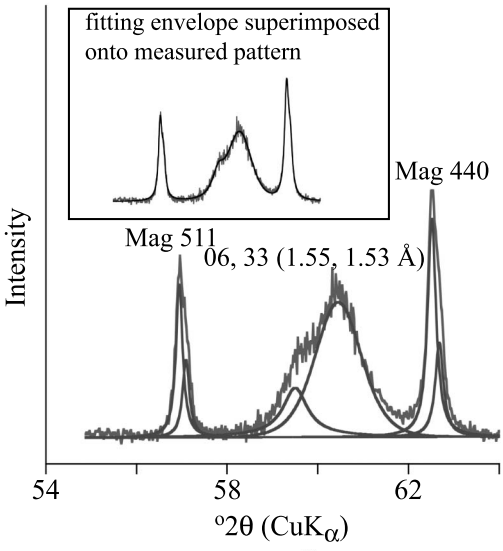

Fig. 1. XRD peaks corresponding to altered smectite 06,33 maxima of experiment 1–13, with curve-fits (black) and measured patterns (grey). The insert shows the fitting envelope superimposed on the experimental pattern. Magnetite peak components have Cu α_1 and α_2 components.

Table 2
Products of series 1 experiments

Experiments	Starting additives	Main reaction products	Trace reaction products
1–1	Fe	Mag, Sm(A)	An, Fe
1–2	Fe + trace of calcite	Mag, Sm(A), An	
1–3	Magnetite + trace of Fe	Mag, Hem, Sm(u)	Qz, An
1–4	Magnetite + traces of calcite and Fe	Mag, Sm(u), An	Hem
1–5	Fe, Magnetite	Mag, Sm(A), An	Hem
1–6	Fe, Magnetite + trace of calcite	Mag, Sm(A), An	Fe, Hem
1–13	Fe	Mag, Sm(A)	Fe
1–14	Fe + trace of calcite	Mag, Sm(A), An	
1–15	Magnetite + trace of Fe	Mag, Hem, Sm(u)	An, Qz
1–16	Magnetite + traces of calcite and Fe	Sm (u), Mag An	
1–17	Fe, Magnetite	Mag, Sm(A)	Qz, Hem
1–18	Fe, Magnetite + trace of calcite	Mag, Sm(A), An	Hem

They are unaltered and altered smectite (SmU, SmA), hematite (Hem), quartz (Qz), and magnetite (Mag) analcime (An).

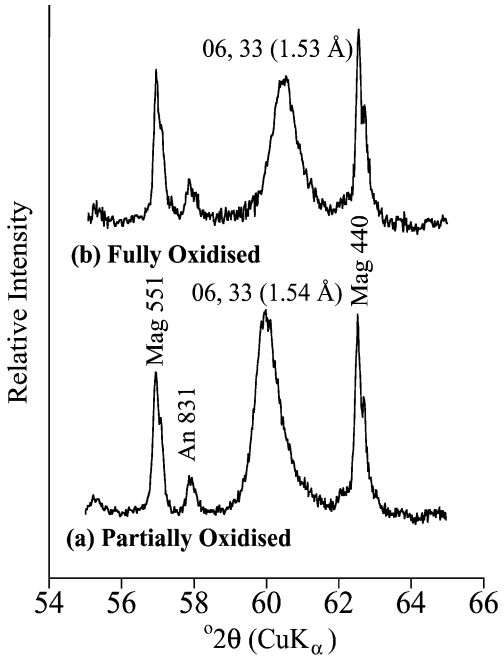

Fig. 2. XRD peaks corresponding to 06,33 of altered smectite in the experiments 1–14 showing *b*-axis contraction during structural Fe oxidation.

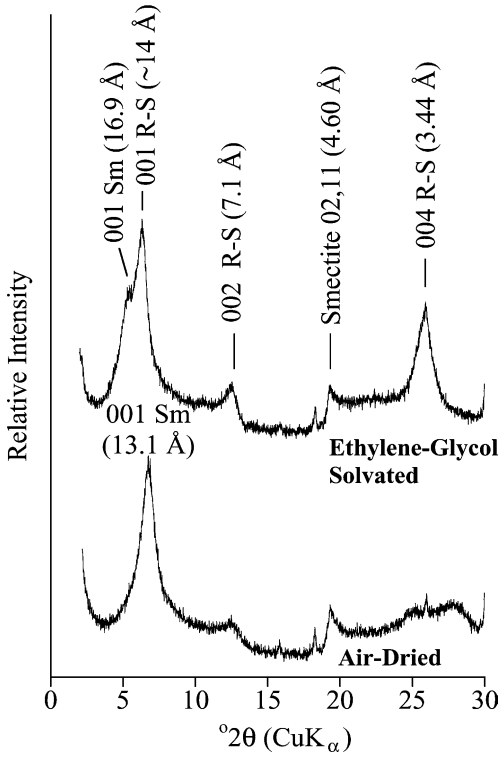

Fig. 3. XRD pattern of a preferred orientation mount of experiments 1–13 in air dry and ethylene glycol solvated states, indicating the presence of normal expanding smectite layers (Sm) and layers which show a reduced swelling capacity on glycolation (R-S).

with montmorillonite (experiments 1–5, 1–6, 1–17, and 1–18), the XRD patterns have only a slightly elevated background at 1.54 Å indicating that the inclusion of smaller amounts of native Fe in starting mixtures results in the less extensive alteration of montmorillonite.

The $d(06,33)$ values of the newly-formed smectite, are similar to those reported by Kohyama et al. (1973) and Badaut et al. (1985) for Fe-rich saponite. Both of these studies found that the Fe(II) present in trioctahedral saponite undergoes rapid oxidation when exposed to air to produce Fe(III)-rich smectite with a trioctahedral $d(06,33)$ value of 1.55 Å (unoxidised) converting to a $d(06,33)$ value of 1.54 Å (partially oxidised) within 1 h. Further exposure of the samples to the atmosphere led to further oxidation with a $d(06,33)$ value of 1.53 Å which is similar to that measured for the material generated in this study (Fig. 2). Other Fe(III)-rich smectite samples reported in the literature have $d(06,33)$ values of ~1.53 Å (Kodama et al., 1988; Sherman and Vergo, 1988) similar to those observed for the oxidised products in this study. However, nontronite (Fe(III) end-member dioctahedral smectite) usually has smaller $d(06,33)$ values (~1.52 Å, e.g., Sherman and Vergo, 1988; Manceau et al., 2000a). The persistence of the 1.55 Å peak in samples when they were exposed to air suggests that a trioctahedral sheet structure is present in addition to the air-sensitive Fe-rich smectite. TEM imaging indicates the presence of 1:1 layers in these samples, but these are dispersed and rarely form extensive crystal regions with a 7 Å layer repeat and therefore do not produce coherent X-ray scattering.

All the Fe(III)-rich smectite alteration products exhibited the same unusual behaviour when subjected to ethylene glycol vapour, in that some layers expand to 17 Å, but much of the sample remains unexpanded at 14–14.4 Å (Fig. 3). In the air-dry state, altered smectite samples have a broad peak at 13–14 Å. After heating to 550 °C, the material collapses to 9.6 Å layer spacing.

3.1.2. XRD analysis of series 2 experiments

On transfer from the hydrothermal vessels into a N_2 atmosphere, the products of series 2 experiments changed colour from light green to brown after only a few minutes, even in the inert N_2 atmosphere. This is attributed to the oxidation of Fe^{2+} (probably in smectite interlayers) to Fe^{3+}. The products consist primarily of clay and magnetite with minor native Fe and lepidocrocite in some cases. Magnetite peaks were observed in all XRD patterns and lepidocrocite peaks were observed in experiments 2–1, 2–2, and 2–3 where high initial concentrations of $FeCl_2$ (18 mM) were included. Native Fe peaks appear in all patterns. Unfortunately lepidocrocite peaks are close to the smectite 06,33 position and such reflections cannot be used with certainty as an indication of octahedral sheet occupancy. However, the positions of the smectite 02,11 reflections in the products of these experiments have a *d*-value of 4.484 Å, suggesting that montmorillonite did not undergo significant alteration to an Fe-rich smectite. However, the XRD patterns suggest that interlayer cation exchange occurred; the $d(001)$ values of

the smectite varied between 14 and 15.4 Å (air-dried state) and expanded to between 16.5 and 17.2 Å on exposure to ethylene glycol. Solute data (Section 3.4) indicate that Na was displaced from interlayers by Fe.

XRD patterns from experiment 2–3 show small peaks at 7.2 and 3.7 Å, consistent with 001 and 002 indexing for a 1:1 layer structure. However, because in 00*l* reflections for Fe-rich chlorite the *l* values are odd and are markedly less intense than those where *l* is an even number, (e.g., Walker and Bish, 1992), there is also the possibility that these peaks correspond to the 002 and 004 chlorite peaks. No *hk* reflections corresponding to this phase were observed and it is therefore not possible to fully identify this phase. A very low intensity peak at ~7 Å was also observed in the pattern from experiment 2–5.

3.2. TEM observations and interpretations

Images of the modified layers of the altered smectite from experiments 1–13 and 1–14 were recorded from grain dispersions viewed by TEM, and are shown in Figs. 4–6. These are structure images, rather than just lattice-fringe

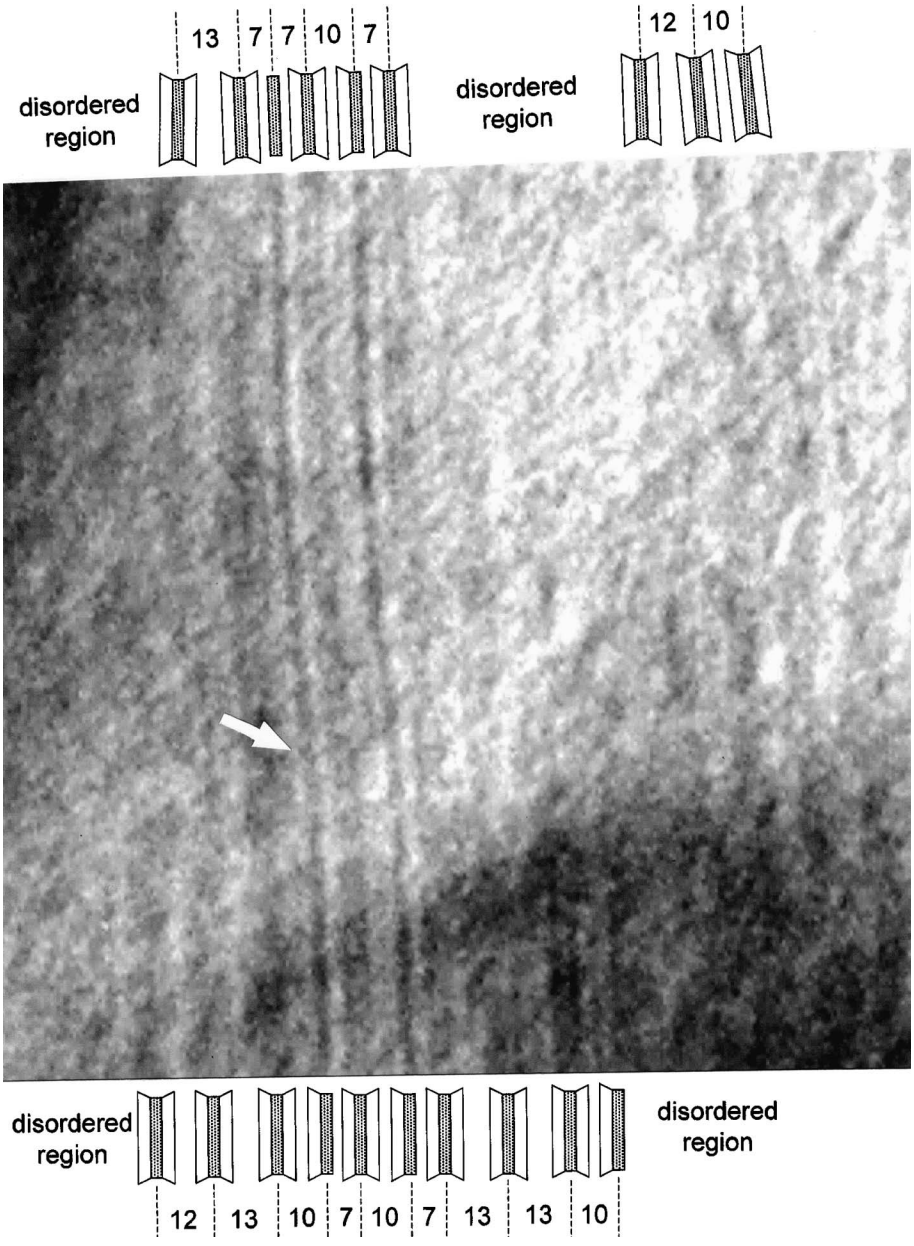

Fig. 4. TEM image of altered, Fe-rich smectite (experiments 1–13). Some packets of 2:1 layers have been retained during the alteration; these have variable interlayer spacings (between 10 and 13 Å) due to variable water loss under the vacuum. Some 2:1 layers have been modified by the loss of the tetrahedral sheet component along one or both sides of the sheet, and these are now held closer (at 7 Å) to adjacent layers. A single octahedral sheet forming a unit of chlorite-type structure (at the top of the image) is seen to become a 1:1 (octahedral–tetrahedral) layer laterally, and the arrow marks the edge dislocation at the termination of the tetrahedral layer. Spacings indicated are in Å units.

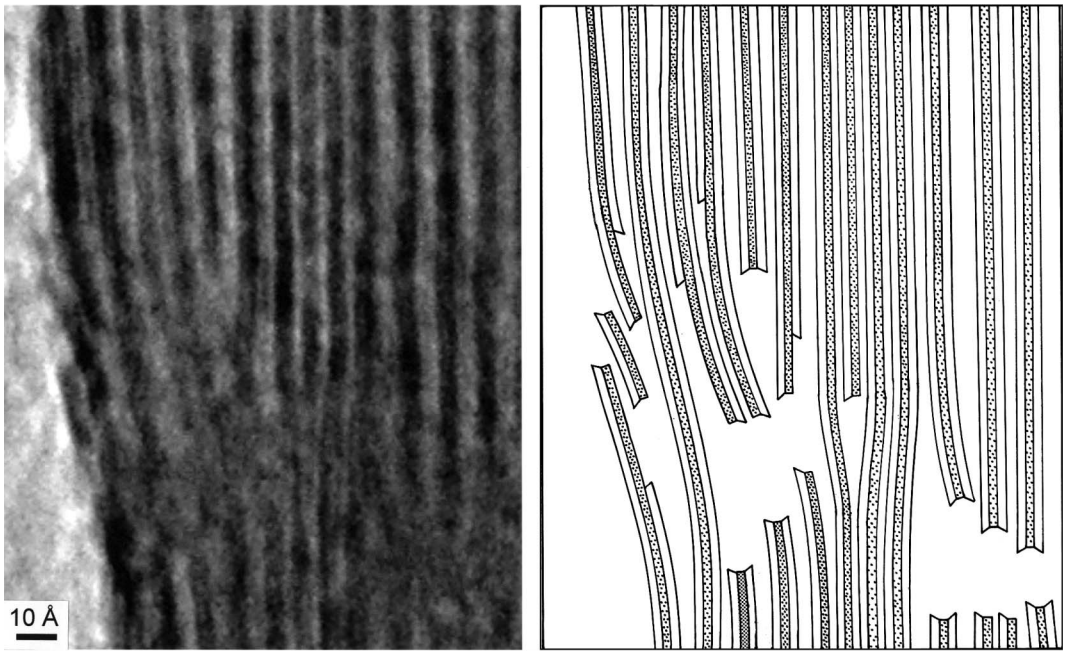

Fig. 5. TEM image and schematic interpretation of altered Fe-rich smectite (experiments 1–14). Many 2:1 sheets have been modified to 1:1 layers by loss of tetrahedral components in the vicinity of edge dislocations that may have facilitated fluid access and the subsequent alteration. Three adjacent 1:1 layers are seen to form a more extensive packet of berthierine or odinite-type structure with a spacing reduced to 7 Å.

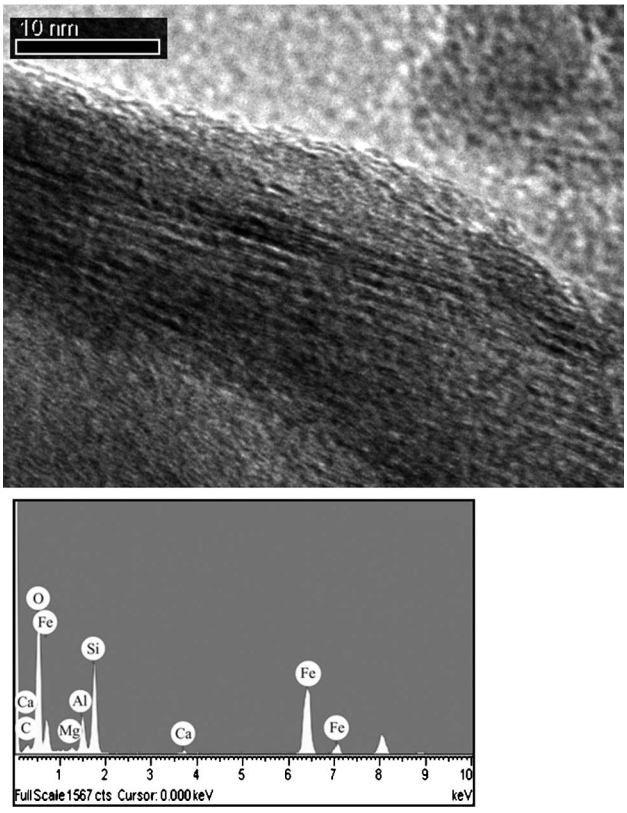

Fig. 6. TEM image of altered Fe-rich smectite (experiments 1–13) showing disrupted layers (see text for details) and an EDS spectrum typical of the altered smectite material.

images, as contrast differences corresponding with the tetrahedral and the octahedral components of the sheets can be distinguished, as can the lower electron density of the inter-sheet planes. Looking along the layer lines at a shallow angle, whilst keeping one eye closed, is the best way to see the features in the images presented.

Regions of disordered structure occur alongside more ordered regions where the structural layers are more clearly defined (Fig. 4); a poorly defined sheet structure appears to continue through these disordered regions, indicative of a poorly crystalline and somewhat disrupted structure, but this is an integral part of the altered smectite and not a structural product of electron beam damage (the whole sample is beam-sensitive and damages badly within 30 s, but with these more disordered regions damaging more quickly). In the regions where the altered structure is reasonably well ordered, packets of 2:1 smectite sheet structure have been retained. However, they now have variable interlayer separations because as water escaped from between the smectite layers under vacuum in the microscope, the structure collapsed to varying degrees; some take up interlayer spacings of ~10 Å (fully collapsed) and others remain partially expanded at 12–13 Å (propped open). The inability of some layers to collapse fully may be because of inhomogeneous cation occupancy of the interlayer space and because of different types and amounts of material introduced into this space during the alteration experiment. It is possible that the more disordered parts may represent 'trapped' regions, where the local chemistry is incompatible with the formation of well-ordered smectite or berthierine.

Table 3
Final solute concentrations (errors are reported to 2 standard deviations)

Experiments	pH (25 °C)	pH (T_{exp})	Fe^{2+} (mM)	2SD	Na^{+} (mM)	2SD	Ca^{2+} (mM)	2SD	Mg^{2+} (mM)	2SD	$SiO_{2(aq)}$ (mM)	2SD	Al^{3+} (mM)	2SD
Series 1														
1–1	7.16	8.45	0.015	0.0001	38.997	0.234	0.088	0.0003	0.013	0.0002	0.79	0.0079	0.06	0.0018
1–2	7.08	8.13	0.013	0.0003	36.816	0.184	0.741	0.0127	0.026	0.0005	0.88	0.0084	0.04	0.0015
1–3	6.74	8.34	0.002	<0.0001	38.423	0.753	0.09	0.0003	0.009	0.0001	1.36	0.0138	0.01	0.0002
1–4	6.60	8.37	0.005	0.0002	37.396	0.322	0.601	0.0055	0.026	0.0003	0.85	0.0279	0.03	0.0007
1–5	7.06	8.37	0.014	0.0001	38.608	0.108	0.085	0.0005	0.009	0.0001	1.34	0.0484	0.04	0.0012
1–6	6.54	8.24	0.007	0.0002	36.816	0.648	0.658	0.0059	0.025	0.0002	1.67	0.047	0.04	0.0006
1–13	6.97	8.47	0.010	0.0001	39.362	0.638	0.072	0.0003	0.021	0.0003	1.34	0.0347	0.06	0.0025
1–14	7.52	8.59	0.006	0.0002	38.916	0.506	0.701	0.0048	0.007	0.0001	0.78	0.0087	0.03	0.0011
1–15	6.91	8.38	0.001	<0.0001	38.736	0.496	0.092	0.0003	0.007	0.0001	1.59	0.0287	0.02	0.0016
1–16	6.19	8.24	0.004	0.0001	37.002	0.429	0.524	0.0083	0.022	0.0003	1.2	0.0329	0.03	0.0005
1–17	6.90	8.26	0.005	<0.0001	37.994	0.456	0.075	0.0004	0.007	0.0001	1.07	0.0103	0.04	0.001
1–18	6.40	8.29	0.013	0.0003	36.335	0.407	0.926	0.0126	0.027	0.0005	0.91	0.0210	0.07	0.0037
Series 2														
2–1	6.27	2.92	7.862	0.076	15.938	0.108	1.008	0.0071	0.441	0.007	0.009	<0.0001	<0.001	—
2–2	5.93	3.23	7.690	0.055	15.914	0.076	1.075	0.0178	0.930	0.011	0.072	<0.0001	<0.001	—
2–3	6.00	3.34	6.279	0.036	15.984	0.192	1.017	0.0045	2.397	0.008	0.437	0.012	0.005	0.0002
2–5	9.68		<0.001	—	12.030	0.070	0.011	0.0002	0.001	<0.0001	0.097	<0.0001	0.005	0.0003
2–6	9.26		<0.001	—	11.401	0.046	0.007	0.0001	0.003	<0.0001	0.744	<0.0001	0.009	0.0003

From these images it is clear that some of the original 2:1 smectite layers have been modified by loss of the tetrahedral sheet along one side of the central octahedral sheet, leaving a 1:1 layer. Thus exposed, octahedral sheets of modified layers have presumably been protonated and are therefore held closer (at ~7 Å) to the tetrahedral base of the adjacent 2:1 sheet by hydrogen bonding. Polar 1:1 layers generated by modification of the 2:1 layers in this way could be considered to be precursors in the development of long-range ordered berthierine or chlorite, depending on their eventual intercalation with the other layers. In support of this alteration mechanism, significant amounts of Si were released into the fluid phase during the experiment (see Table 3). A similar style of alteration (i.e. loss of tetrahedral silicon units from 2:1 layers) has also been reported from TEM imaging of biotite altering to chlorite by Veblen and Ferry (1983). The image in Fig. 4 also shows a further aspect of the partial alteration of the smectite: one of the 1:1 layers is also beginning to lose its remaining tetrahedral sheet, so that the 1:1 layer passes laterally into a single octahedral sheet, and an edge dislocation (which has propagated through the structure) marks the termination of the tetrahedral layer. Therefore, it seems that the original 2:1 layers can be modified by tetrahedral loss from both sides, and it is likely that this modification could begin to happen at different positions simultaneously throughout the layer. The end-product single octahedral layer seen in this figure forms one unit of chlorite-type structure with adjacent smectite layers. It seems likely that the alteration proceeded in both directions along the layers, with the fluid moving along the planar interlayer pathways in the smectite. Initially, dissolved Fe could have migrated easily throughout the entire smectite interlayer space, then, commensurate with the breaching of the tetrahedral layers and the extraction of Si into solution, Fe^{2+} will have diffused into the central octahedral layer, replacing the Al (di-octahedral occupancy), and changing the structure to a predominantly tri-octahedral occupancy. Indeed, all the altered smectite grains analysed by TEM-EDS were observed to be very Fe-rich (see Fig. 6). Although the exact chemistry of the 1:1 and single octahedral sheets in Fig. 4 is too small to determine individually by TEM-EDS, it is likely that they are Fe-rich with compositions close to berthierine or odinite. The single octahedral layer product is probably Fe-hydroxide, and if so will be tightly hydrogen bonded to the basal tetrahedral oxygens of the neighbouring sheets. It is interesting to note that the newly generated octahedral components visible in Fig. 4 have a darker contrast relative to the octahedral components of retained 2:1 layers; although difficult to prove, this may be due to the higher electron density of Fe relative to Al, suggesting that more Fe was able to diffuse into these 'exposed' layers.

The TEM image shown in Fig. 5 illustrates a region in the altered smectite with many edge dislocations. Many of the original 2:1 smectite layers appear to have been modified by the loss of a tetrahedral layer along one side. The 2:1 sheets modified to 1:1 sheets are recognised by their

~7 Å spacings to adjacent sheets, while the smectite-like packets remaining have spacings of ~10 Å. In this image a group of three adjacent 1:1 layers have begun to form a more extensive 7 Å berthierine-type structure. The loss of tetrahedral units along individual layers appears to have proceeded in a direction away from the edge dislocations that may have been present in the original smectite and therefore may have facilitated fluid access to the interior of grains and promoted the subsequent alteration.

The grain shown in Fig. 6, appears at first sight to consist predominantly of smectite-type layers with spacings of about 10 Å. However, closer inspection reveals that these layers have numerous disruptions and edge dislocations. Where the layers are disrupted (or sometimes broken through) they approach adjacent layers more closely at approximately 7 Å. The spacings of layers in this image of altered smectite range from 10 Å down to 7 Å, with the smaller spacings occurring as a pinching together of the sheets at different points. This is interpreted as the effect of locally formed hydrogen bonding between sheets where tetrahedral side components are being removed. The only way such layers can approach one another closer than 10 Å is if there are no interlayer cations and hydrogen bonds form instead. In effect the layers are being 'spot-welded' together by the hydrogen bonding. It is likely that this incipient alteration of the smectite to a more tightly bonded layer structure has occurred throughout the bulk of the smectite in the experiment, and is probably responsible for the observed change in physical behaviour of the bulk product. Prior to reaction the smectite behaved as normal expandable clay, but after the alteration experiment the expansion by ethylene glycol was observed to be much impaired (see Fig. 3). It is likely that as the ethylene glycol enters between layers at the edges of grains, any hydrogen-bonded patches encountered will prevent the further expansion of that particular layer space. If this occurs at some point within many layers close to the grain edge, then the ethylene glycol will be prevented from migrating into the bulk of the grain. Any volume converted to berthierine or chlorite will similarly not be expanded by glycol. Since the alteration of the smectite in the experiment would have occurred primarily around grain edges (or along existing edge dislocations as shown), the hydrogen-bonded units thus formed are likely to arrest any glycolation close to its entry point.

3.3. FT-IR analysis

For series 1 experiments where magnetite was added as the main source of Fe, little change in band position with respect to the original montmorillonite was observed. The most evident difference is that the AlAlOH band (912 cm^{-1}) of the products had a reduced intensity relative to the starting material.

For experiments where significant quantities of native Fe were included in the starting mixtures the maxima of OH-stretching bands were centred at 3555 cm^{-1} (as opposed to 3629 cm^{-1} in the starting material). Such bands have been attributed to dioctahedral Fe(III)Fe(III)OH groupings in nontronite and ferruginous smectite (Goodman et al., 1976; Madejová et al., 1994; Russell and Fraser, 1994; Komadel et al., 1999; Fialips et al., 2002b).

In these experiments, OH-deformation bands are absent relative to the starting montmorillonite and are replaced by low-intensity bands at ~818, 735, and 670 cm^{-1} (Fig. 7). Bands at ~820 cm^{-1} have previously been assigned to Fe(III)Fe(III)OH groupings (Stubican and Roy, 1961; Farmer, 1964; Goodman et al., 1976; Russell and Fraser, 1994; Madejová et al., 1994; Komadel et al., 1995; Karakassides et al., 2000; Vantelon et al., 2001; Fialips et al., 2002a). The band at 735 cm^{-1} has previously been attributed to Si–O–(IV)Al vibrations in trioctahedral smectite (Farmer, 1974). The band at 670 cm^{-1} appears to be due to out of plane Fe(III)–O vibrations (Russell and Fraser, 1994).

The overall Si–O stretching bands of the samples from series 1 experiments are at a slightly lower frequency (~1024 cm^{-1}) compared to the montmorillonite starting material (~1038 cm^{-1}) and are within the reported range for nontronite (1000–1029 cm^{-1}, Goodman et al., 1976; Fialips et al., 2002a). The frequencies of Si–O bands generally decrease with increasing Al substitution for Si in sheet silicates (Russell and Fraser, 1994) which in conjunction with the weak Si–O–(IV)Al lattice vibration band at 735 cm^{-1}, suggest that the altered smectite has tetrahedral sheet occupancy which is more like nontronite or saponite than montmorillonite, with significant Al substitution for Si.

In summary, all of these features indicate that the altered smectite is Fe(III)-rich. Although some features of

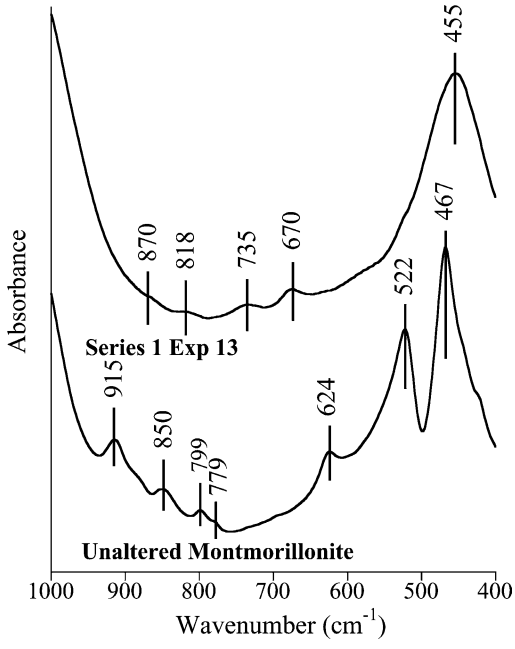

Fig. 7. FT-IR spectra (OH-deformation region) of altered smectite experiments 1–13 and montmorillonite starting material.

the spectra suggest a dioctahedral-type sheet (OH-stretching, several OH-bending bands), others are more typical of a trioctahedral structure (bands at 735 and 455 cm^{-1}). This is probably due to structural modification of octahedral sheets produced by Fe oxidation.

FT-IR spectra given by smectite in the products of the series 2 experiments show only subtle changes from the original montmorillonite spectrum. These changes are most pronounced in the spectra of the experiments conducted at 250 °C as OH-deformation bands of lower intensity than those of the montmorillonite starting material. A low intensity component at ~3550 cm^{-1} is detectable in experiments 2–3 and 2–6 indicating that Fe(III)Fe(III)OH bands are present and that minor alteration may have occurred.

3.4. Solute analysis

Dissolved Fe was detected in solutions from all experiments, except 2–5 and 2–6 (Table 3). In series 1 experiments, concentrations of dissolved Fe ranged from 0.001 to 0.015 mM with higher concentrations generally occurring in experiments which had more native Fe in the starting mixtures. The high concentrations of Fe (6.3–7.9 mM) were present in experiments where $FeCl_2$ was added to starting mixtures at an initial concentration of 18 mM.

Exchangeable cation data indicate that the displacement of all interlayer cations to solution would produce the following solute concentrations: Na^+, 16 mM; Ca^{2+}, 0.9 mM; and Mg^{2+}, 0.06 mM. Dissolved Fe displaced most (if not all) of the interlayer Na^+ in the series 2 experiments where it was added in concentrations of 18 mM (2–1 to 2–3). Initial $FeCl_2$ concentrations of 4.5 mM in experiments 2–5 and 2–6 resulted in partial release of Na^+ to solution, since this Fe^{2+} concentration is sufficient to satisfy only half of the layer charge deficit of Kunipia-F montmorillonite.

In the series 1 experiments, higher Ca^{2+} concentrations were produced in the experiments where calcite was added. In the experiments where calcite was not added, the concentrations of Ca^{2+} were not sufficiently high to indicate that there was total release from smectite interlayers. The Ca^{2+} concentrations measured in solutions from experiments 2–1, 2–2, and 2–3 exceed those from the first series of experiments, indicating that dissolved Fe^{2+} was more effective than Na^+ at displacing interlayer Ca^{2+} under hydrothermal conditions. Experiments where initial dissolved Fe concentrations were 4.5 mM (experiments 2–5 and 2–6) led to only partial displacement of Ca^{2+} to solution.

The concentrations of Mg^{2+} measured in solutions from the first series of experiments varied between 0.007 and 0.026 mM. No clear trends can be observed between measured Mg^{2+} concentrations and the mineral assemblages produced. This indicates that Mg remained largely as an interlayer cation or was incorporated into octahedral sheets. Concentrations measured in the solutions from the series 2 experiments showed an increase with reaction temperature. The concentrations of Mg^{2+} in the experiments with lower initial concentrations of $FeCl_2$ (experiments 2–5 and 2–6) indicate that there was partial displacement of interlayer Mg to solution. The addition of high concentrations of $FeCl_2$ to the starting mixtures produced Mg^{2+} concentrations which exceed that expected from cation exchange alone (0.4 and 2.4 mM) indicating significant loss of Mg from the octahedral sheets of the 2:1 layers. This suggests that Mg on octahedral sites in the original montmorillonite structure could have been replaced by Fe.

The amount of $SiO_{2(aq)}$ and Al^{3+} released to solution was higher in the series 1 experiments, where smectite alteration was more extensive and dissolved Na concentrations exceeded those present at the start of the experiments. In the series 2 experiments, dissolved Si and Al concentrations increased with higher temperatures. Dissolved Si may be present due to dissolution of the minor amounts of quartz and cristobalite present in the starting material, as well as clay mineral dissolution.

The pH values of supernatant fluids (measured at room temperature) were generally between 6 and 7, apart from experiments 2–5 and 2–6, where they were 9.3 and 9.7 units, respectively (Table 3). The pH values calculated at reaction temperatures for series 1 experiments ranged from 8.1 to 8.5 units and those for series 2 experiments 1–3 were in the range of 2.9–3.3 units. Higher pH values in the series 1 experiments were produced where native Fe was present (these experiments also produced higher dissolved Fe concentrations). The experiments with added calcite (which led to significant smectite alteration to analcime) did not give significantly different pH values from those without calcite. The pH values in the second series of experiments were highest where Fe concentrations were lowest (experiments 2–5 and 2–6).

Table 4
Calculated saturation indices

Experiment	Magnetite $\log f O_{2(g)}$		Quartz
	−43.65	−35.30	
Series 1			
1–1	18.934	23.109	−1.080
1–2	17.924	22.009	−0.986
1–3	15.509	19.684	−0.807
1–4	17.002	21.176	−1.017
1–5	18.288	22.463	−0.822
1–6	16.695	20.870	−0.690
1–13	18.520	22.695	−0.858
1–14	18.431	22.606	−1.137
1–15	15.259	19.434	−0.751
1–16	15.891	20.066	−0.835
1–17	16.401	20.576	−0.888
1–18	17.714	21.889	−0.967
Series 2			
2–1	−18.136	−13.821	−1.803
2–2	−16.011	−5.691	−1.426
2–3	−3.915	0.260	−1.154

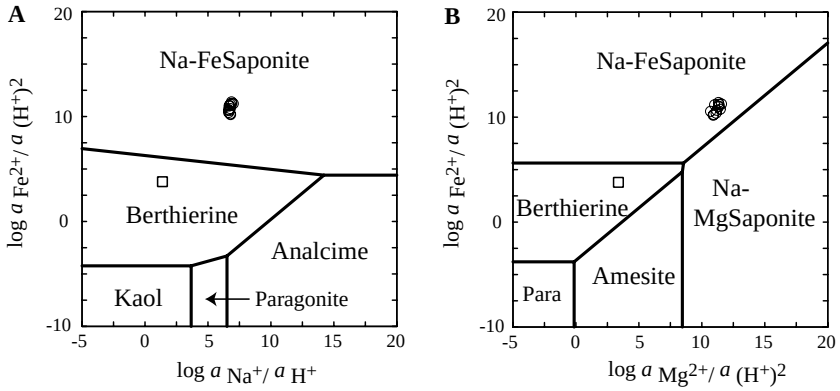

Fig. 8. Plots of solute activity ratios on logarithmic activity diagrams ($T = 250$ °C, $P = P_{sat}$) for the systems Al_2O_3–FeO–Na_2O–SiO_2–H_2O (A) and Al_2O_3–FeO–MgO–Na_2O-SiO_2–H_2O (B). In both plots, $\log a_{SiO_{2(aq)}} = -3$, $a_{H_2O} = 1$ and in (B), $\log(a_{Na^+}/a_{H^+}) = 5$. Circles denote series 1 experiments, the square corresponds to experiment 2–3.

3.5. Thermodynamic interpretation of experimental data

The same predictions of solute activities were obtained when $f_{O_{2(g)}}$ was set at H_2–H_2O equilibrium or magnetite-hematite equilibrium. Calculated saturation indices indicate that the solutions were supersaturated in magnetite, more so for higher $f_{O_{2(g)}}$ values (Table 4). All experiments were undersaturated with respect to quartz.

For series 1 experiments, data points of solute activity ratios on logarithmic diagrams in the systems Al_2O_3–FeO–Na_2O–SiO_2–H_2O (Fig. 8A) and Al_2O_3–FeO–MgO–Na_2O–SiO_2–H_2O (Fig. 8B) plot in the Fe(II)-saponite stability field. On the same diagrams, experiment 2–3 plots in bertherine stability fields. Although the diagrams include Na^+-exchanged Fe(II) saponite, the solute activities would also plot in the hypothetical Fe^{2+}-exchanged Fe(II) saponite stability field (see Wilson et al., 2006). If smectite minerals were excluded from the phase diagrams, the solute activities would plot within the field for Fe chlorite (see Wilson et al., 2006).

4. Discussion and conclusions

The oxidation of native Fe to produce magnetite is in agreement with thermodynamic models. Wilson et al. (2006) suggest that either green-rust or magnetite could be produced from the oxidation of native Fe. It is probably the case that green rust is metastable with respect to magnetite under the conditions of the experiments. It is not possible to show unequivocally that equilibrium was attained in these experiments. This would require the demonstration of phase reversal across a univariant phase boundary or, as some authors argue, by showing solute activities converging from under and over-saturation to produce a univariant phase boundary in activity space (Aja and Rosenberg, 1992). However, the alteration of montmorillonite to Fe-rich smectite is predicted by the thermochemical models presented by Wilson et al., 2006, showing that Fe-rich systems at low $f_{O_{2(g)}}$ and neutral to alkaline pH conditions are more likely to result in montmorillonite undergoing alteration predominantly to Fe(II)-smectite. The XRD, FT-IR, and TEM-EDS results confirm this prediction, showing that the major alteration product was an Fe(II)-rich smectite (which oxidised to Fe(III)-rich smectite upon contact with the atmosphere). The formation of individual 1:1 layers was observed by TEM, suggesting that these are produced when tetrahedral silica is removed from one or both sides of disrupted smectite layers. Experiment 2–3 plots in berthierine stability fields, which is supported by XRD evidence for a 7 Å layer phase. The lack of major alteration in experiment 2–3 compared to series 1 experiments suggests that the alteration of montmorillonite to Fe-rich smectite is less kinetically constrained than the alteration of smectite to a 1:1 mineral. The experiments also show that native Fe is more effective than magnetite in providing Fe(II) for montmorillonite alteration.

In the series 1 experiments, TEM evidence gives insights to the transformation mechanism of montmorillonite alteration. It is clear that loss of tetrahedral silica occurs from some sheets to produce lateral transitions of smectite to 1:1 layers and that this process can continue to eventually produce hydroxide sheets. The lack of a 7 Å peak in XRD patterns indicates that the modified 7 Å layers are too dispersed throughout the smectite to coherently diffract X-rays. However, these 1:1 modifications are sufficiently numerous to impair the overall swelling property of the bulk of Fe-smectite alteration product. In series 2 experiments, there is alteration to produce a 7 Å berthierine-like phase that is detectable using XRD, with the unaltered montmorillonite remaining and retaining the capacity to expand when glycolated. The plots of solute activities on logarithmic activity diagrams (Fig. 8) suggest that the alteration of montmorillonite to a 1:1 phase in the series 2 experiments was more extensive because it was thermodynamically more favourable than in series 1 experiments. The production of 1:1 layers in the series 1 experiments, in contrast, appears to be more localised as the conditions generally favoured the formation of Fe(II)-rich smectite. The dispersed 1:1 layers produced in the series 1 experiments could be interpreted as showing that the experiments

proceeded towards equilibrium, but did not fully attain equilibrium, i.e., they are remnants of partially altered montmorillonite layers. However, demonstrating that a given fluid-clay system achieved equilibrium is likely to continue to prove very difficult, although this study shows that considering approximate (meta)stability fields for clay minerals may give an indication of the direction that mineral alteration pathways may proceed.

Some of the results of our experiments are similar to those conducted by Guillaume et al. (2003). In their study, reacting mixtures of bentonite, native Fe and magnetite with NaCl and $CaCl_2$ solutions for up to 9 months at 300 °C, resulted in the production of high-charge trioctahedral smectite and the native Fe was converted to magnetite. However, the smectite produced in their experiments expanded normally after treatment with ethylene glycol and they also produced chlorite in experiments when a plate of Fe was present. Guillaume et al. (2004) produced an Fe(II) smectite by reacting bentonite with magnetite and hematite at 300 °C over a period of 9 months. However, unlike the Fe-rich smectite produced in this study, theirs was expanded by ethylene glycol solvation, although it did not expand fully when the original interlayer configuration was altered by K-saturation prior to glycolation.

Another difference between the results of our study and that of Guillaume et al. (2004) is that there was a lack of montmorillonite alteration in our experiments which included magnetite in the starting mixtures. This may be due to our experimental conditions being less extreme (250 °C, ~3 months reaction time as opposed to 300 °C, up to 9 months reaction time).

The oxidation of Fe(II) in the Fe-rich smectite produced in this study upon exposure to air may have involved the disruption of structural OH. Kohyama et al. (1973) suggested that the oxidation of Fe(II)-saponite may occur via the dehydroxylation of octahedral sheets. The oxidation of Fe(II) appears to have resulted in disruption of layer structures, to produce material which may not have simple end-member di- or trioctahedral occupancy. However, any deprotonation of octahedral layers appears not to have affected the efficacy of the 7 Å H-bonded layer repeats generated in the transformation.

The enhanced alteration of montmorillonite to analcime in the presence of calcite may be due to the effect that calcite dissolution had on pH. The dissolution of calcite may have increased the pH of the solutions during the early stages of the experiments before significant Fe^{2+} activities developed, resulting in solute activities initially coinciding with analcime stability fields.

5. Implications for high level radioactive waste disposal

The experiments show that Fe-rich smectite (possibly with some dispersed 7 Å layers) is the most likely alteration product at steel canister–bentonite interface in HLW repositories and that native Fe is more effective in altering the montmorillonite than magnetite. Experiments suggest that montmorillonite is less likely to alter to Fe-rich smectite after canister corrosion has ceased. The alteration of smectite to predominantly 1:1 sheet silicates via silica loss is only to be expected if pore water pH values are relatively low. The function of the bentonite backfill in a HLW repository is only likely to be compromised if montmorillonite is altered to a non-swelling sheet silicate or Fe(II)-rich smectite with impaired swelling properties. Since most repository designs include quartz sand–bentonite mixtures, pore waters may proceed towards silica saturation at the expense of quartz dissolution as well as smectite dissolution. Therefore the loss of tetrahedral units from smectite layers in a repository (resulting in increased hydrogen bonding between layers and impaired swelling) may be less prevalent than that produced in our experiments. Given its desirable swelling and adsorption properties, bentonite is therefore a good choice of backfill material, providing measures are taken to minimise the potential for impaired swelling properties to develop. In systems where steel waste canisters are used, such measures may include: (1) ensuring that excess silica is available in the bentonite backfill (most designs already include quartz sand) and (2) using steel that is relatively more resistant to corrosion, or that has surfaces which are oxidised prior to bentonite emplacement. In light of the results of this paper, other metals, such as titanium, may be considered as an alternative to iron for use as waste containers. It is clear that in order to maximise the effectiveness of a multiple-barrier system to encapsulate nuclear waste (thereby also maximising repository safety), predictions of the chemical and engineering consequences of each possible combination of available materials have to be carefully considered.

Acknowledgements

The authors thank Tony Kemp and P. Chung Choi (Department of Earth Sciences, University of Bristol) for assistance in ICP-AES and ICP-MS analysis; Fred Wheeler, Mike Dury, and Phil Boyd (University of Bristol) for constructing the hydrothermal apparatus and Martin Gill (Natural History Museum) for assistance with XRD analysis. Part of this work was completed whilst the principal author was NERC (CASE) funded Ph.D. student. The authors also wish to thank the Japan Nuclear Cycle Development Institute (JNC) and Quintessa, for financial assistance. O.Vidal, two anonymous reviewers and the Associate Editor, E.H. Oelkers, are thanked for constructive reviews.

Associate editor: Eric H. Oelkers

References

Aja, S.U., Rosenberg, P.E., 1992. The thermodynamic status of compositionally variable clay minerals—a discussion. *Clays Clay Miner.* **40**, 292–299.

Badaut, D., Besson, D., Decarreau, A., Rautureau, R., 1985. Occurrence of a ferrous trioctahedral smectite in recent sediments of Atlantis II Deep, Red Sea. *Clay Miner.* **20**, 389–404.

Batchelder, M., Cressey, G., 1998. Rapid, accurate phase quantification of clay-bearing samples using a position-sensitive X-ray detector. *Clays Clay Miner.* **46**, 183–194.

Bergaya, F., Vayer, M., 1997. CEC of Clays, measurement by adsorption of a copper ethylenediamine complex. *Appl. Clay Sci.* **12**, 275–280.

Bethke, C.M., 1996. *Geochemical Reaction Modeling*. Oxford University Press, Oxford.

Cuadros, J., Linares, J., 1996. Experimental kinetic study of the smectite-to-illite transformation. *Geochim. Cosmochim. Acta* **60**, 439–453.

Decarreau, A., Bonnin, D., 1986. Synthesis and crystallogenesis at low temperature of Fe(III) smectites by evolution of coprecipitated gels; experiments in partially reducing conditions. *Clay Miner.* **21**, 861–877.

Farmer, V.C., 1964. Infrared absorption of hydroxyl groups in kaolinite Spectra of Minerals. *Science* **145**, 1189–1190.

Farmer, V.C., 1974. The layer silicates. In: Farmer, V.C. (Ed.), *The Infra-Red Spectra of Minerals*. Mineralogical Society, London, pp. 331–364.

Fialips, C.-I., Huo, D., Yan, L., Wu, J., Stucki, J.W., 2002a. Effect of Fe oxidation state on the IR spectra of Garfield nontronite. *Am. Mineral.* **87**, 630–641.

Fialips, C.-I., Huo, D., Yan, L., Wu, J., Stucki, J.W., 2002b. Infrared study of reduced-reoxidised ferruginous smectite. *Clays Clay Miner.* **50**, 455–469.

Glaeser, R., Méring, J., 1968. Homogeneous hydration domains of the smectites. *CR Seances Acad Sci. Paris* **267**, 436–466.

Goodman, B.A., Russell, J.D., Fraser, A.R., Woodhams, F.W.D., 1976. A mossbauer and infrared spectroscopic study of the structure of nontronite. *Clays Clay Miner.* **24**, 53–59.

Guillaume, D., Neaman, A., Cathelineau, M., Mosser-Ruck, R., Peiffert, C., Abdelmoula, M., Dubessy, J., Villiéras, F., Baronnet, A., Michau, N., 2003. Experimental synthesis of chlorite from smectite at 300 °C in the presence of metallic Fe. *Clay Miner.* **38**, 281–302.

Guillaume, D., Neaman, A., Cathelineau, M., Mosser-Ruck, R., Peiffert, C., Abdelmoula, M., Dubessy, J., Villiéras, F., Michau, N., 2004. Experimental study of the transformation of smectite at 80 and 300 °C in the presence of Fe oxides. *Clay Miner.* **39**, 17–34.

Harder, H., 1976. Nontronite synthesis at low temperatures. *Chem. Geol.* **18**, 169–180.

Harder, H., 1978. Synthesis of iron layer silicate minerals under natural conditions. *Clays Clay Miner.* **26**, 65–72.

Helgeson, H.C., 1969. Thermodynamics of hydrothermal systems at elevated temperatures and pressures. *Am. J. Sci.* **267**, 729–804.

Huang, N.-L., Longo, J.M., Pevear, D.R., 1993. An experimentally derived kinetic model for smectite to illite conversion and its use as a geothermometer. *Clays Clay Miner.* **41**, 162–177.

Kamei, G., Oda, C., Mitsui, S., Shibata, M., Shinozaki, T., 1999. Fe(II)-Na ion exchange at interlayers of smectite: adsorption-desorption experiments and a natural analogue. *Eng. Geol.* **54**, 15–20.

Karakassides, M.A., Gournis, D., Simopoulos, T., Petridis, D., 2000. Mossbauer and infrared study of heat-treated nontronite. *Clays Clay Miner.* **48**, 68–74.

Kodama, H., De Kimpe, C.R., Dejou, J., 1988. Ferrian saponite in a gabbro saprolite at Mont Blanc Magantic, Quebec. *Clays Clay Miner.* **36**, 102–110.

Kohyama, N., Shimoda, S., Sudo, T., 1973. Iron-rich saponite ferric and ferrous forms. *Clays Clay Miner.* **21**, 229–237.

Komadel, P., Madejova, J., Stucki, J.S., 1995. Reduction and reoxidation of nontronite, questions of reversibility. *Clays Clay Miner.* **43**, 105–110.

Komadel, P., Madejova, J., Stucki, J.S., 1999. Partial stabilisation of FeII in reduced ferruginous smectite by Li fixation. *Clays Clay Miner.* **47**, 458–465.

MacEwan, D., Wilson, M., 1980. Interlayer and intercalation complexes of clay minerals. In: Brindley, G.W., Brown, G. (Eds.), *Crystal Structures of Clay Minerals and Their X-ray Identification*. Mineralogical Society, London, pp. 197–248.

Madejová, J., Komadel, P., Cicel, B., 1994. Infrared study of octahedral site populations in smectites. *Clay Miner.* **29**, 319–326.

Madsen, F.T., 1998. Clay mineralogical investigations related to nuclear waste disposal. *Clay Miner.* **33**, 109–129.

Manceau, A., Lanson, B., Drits, V.A., Chateigner, D., Gates, W.P., Wu, J., Huo, D., Stucki, J.W., 2000a. Oxidation-reduction mechanism of iron in dioctahedral smectites,1. Crystal chemistry of oxidised reference nontronites. *Am. Mineral.* **85**, 133–152.

Moore, D.M., Reynolds, R.C., 1997. *X-ray Diffraction and the Identification and Analysis of Clay Minerals*. Oxford University Press, Oxford.

Müller-Vonmoos, M., Kahr, G., Bucher, F., Madsen, F.T., Mayor, P.-A., 1991. Untersuchungen zum verhalten von bentonit in kontakt mit magnetit und eisen under Endlagerbedingungen. NTB 91-14. Nagra, Hardstrasse 73, Schweiz, CH-5430 Wettingen.

Russell, J., Fraser, A.R., 1994. Infrared Methods. In: Wilson, M.J. (Ed.), *Clay Mineralogy Spectroscopic and Chemical Determinative Methods*. Chapman and Hall, London.

Sherman, D.M., Vergo, N., 1988. Optical (diffuse reflectance) and Mossbauer spectroscopic study of nontronite and related Fe-bearing smectites. *Am. Mineral.* **73**, 1346–1354.

Stubican, V., Roy, R., 1961. A new approach to assignment of infra-red adsorption bands in layer structure silicates. *Z. Kristallogr.* **15**, 200–214.

Vantelon, D., Pelletier, M., Michot, L.J., Barres, O., Thomas, F., 2001. Fe, Mg and Al distribution in the octahedral sheet of montmorillonites. An infrared study in the OH-bending region. *Clay Miner.* **36**, 369–379.

Veblen, D.R., Ferry, J.M., 1983. A TEM study of the biotite-chlorite reaction and comparison with petrologic observations. *Am. Mineral.* **68**, 1160–1168.

Walker, J.R., Bish, D.L, 1992. Application of rietveld refinement techniques to a disordered-IIb Mg-chamosite. *Clays Clay Miner.* **40**, 319–322.

Whitney, G., Northrop, H.R., 1988. Experimental investigation of the smectite to illite reaction, dual reaction mechanism and oxygen isotope systematics. *Am. Mineral.* **73**, 77–90.

Wilson, J., Savage, D., Cuadros, J., Shibata, M., Ragnarsdottir, K.V., 2006. The effect of iron on montomorillonite stability. (I) Background and thermodynamic considerations. *Geochim. Cosmochim. Acta* **70**, 306–322.

Wolery, T., 1996. EQ3/6 Database. Lawrence Livermore National Laboratory, USA.